

1 **Pleiotropic effect of Lactoferrin in the prevention and treatment of COVID-19 infection:**
2 ***randomized clinical trial, in vitro and in silico preliminary evidences***

3

4 Elena Campione,^{1*} Caterina Lanna,¹ Terenzio Cosio,¹ Luigi Rosa,² Maria Pia Conte,² Federico
5 Iacovelli,³ Alice Romeo,³ Mattia Falconi,³ Claudia Del Vecchio,⁴ Elisa Franchin,⁴ Maria Stella
6 Lia,⁵ Marilena Minieri,⁵ Carlo Chiamonte,⁶ Marco Ciotti,⁷ Marzia Nuccetelli,⁸ Alessandro
7 Terrinoni,⁵ Iliaria Iannuzzi,⁹ Luca Coppeda,⁹ Andrea Magrini,⁹ Nicola Moricca,¹⁰ Stefano Sabatini,¹⁰
8 Felice Rosapepe,¹¹ Pier Luigi Bartoletti,¹² Sergio Bernardini,⁸ Massimo Andreoni,¹³ Piera
9 Valenti,^{2§} Luca Bianchi^{1§}

10 ¹Dermatology Unit, University of Rome “Tor Vergata”, Rome, 00133, Italy.

11 ²Department of Public Health and Infectious Diseases, University of Rome “La Sapienza”, 00185,
12 Italy.

13 ³Department of Biology, Structural Bioinformatics Group, University of Rome “Tor Vergata”,
14 Rome, 00133, Italy.

15 ⁴Department of Molecular Medicine, University of Padova, 35122 Padova, Italy.

16 ⁵Department of Experimental Medicine, Tor Vergata University Hospital, Rome, 00133, Italy.

17 ⁶Departement of statistics, University of Rome Tor Vergata, Rome, 00133, Italy.

18 ⁷Virology Unit, Tor Vergata University Hospital, Rome, 00133, Italy.

19 ⁸Laboratory Medicine, Department of Experimental Medicine and Surgery, Tor Vergata University
20 Hospital,

21 ⁹Occupational Medicine Department, University of Rome "Tor Vergata", Rome, 00133, Italy.

22 ¹⁰Villa dei Pini Hospital, Anzio (RM), Italy.

23 ¹¹Pineta Grande Hospital, Caserta, Italy

24 ¹²Fimmg provincial, Rome, Italy

25 ¹³Infectious Disease Unit, Tor Vergata University Hospital, Rome, 00133, Italy

26 [§]Those authors equally contributed as senior authors

27 **Correspondence:** elena.campione@uniroma2.it; campioneelena@hotmail.com

28

29 ABSTRACT

30 The current treatments against SARS-CoV-2 have proved so far inadequate. A potent antiviral drug
31 is yet to be discovered. Lactoferrin, a multifunctional glycoprotein, secreted by exocrine glands and
32 neutrophils, possesses an antiviral activity extendable to SARS-Cov-2.

33 We performed a randomized, prospective, interventional study assessing the role of oral and intra-
34 nasal lactoferrin to treat mild-to-moderate and asymptomatic COVID-19 patients to prevent disease
35 evolution. Lactoferrin induced an early viral clearance and a fast clinical symptoms recovery in
36 addition to a statistically significant reduction of D-Dimer, Interleukin-6 and ferritin blood levels.
37 The antiviral activity of lactoferrin related to its binding to SARS-CoV-2 and cells and *protein-*
38 *protein docking methods*, provided the direct recognition between lactoferrin and spike S, thus
39 hindering the spike S attachment to the human ACE2 receptor and consequently virus entering into
40 the cells.

41 Lactoferrin can be used as a safe and efficacious natural agent to prevent and treat COVID-19
42 infection.

43 **KEYWORDS:** lactoferrin, COVID-19, SARS-CoV2

44

45 INTRODUCTION

46 In December 2019, in Whuan, China, a cluster of pneumonia cases was observed. This cluster was
47 related to a novel member of *Betacoronavirus*, named SARS-CoV-2, possessing more than 80%
48 identity to SARS-CoV and 50% to the MERS-CoV^{1,2}. Coronavirus are spherical, enveloped viruses
49 possessing a single-strand, positive-sense RNA genome ranging from 26 to 32 kilobases in length³.
50 Their genome encodes 16 non-structural proteins⁴, accessory proteins⁵ and 4 essential structural
51 proteins, namely spike S glycoprotein, small envelope protein, matrix protein, and nucleocapsid
52 protein⁶. Homotrimeric S glycoprotein, possessing N-linked glycans, is located on the envelope and
53 comprises two subunits (S1 and S2) in each spike monomer⁷. As homotrimers of S glycoproteins
54 are exposed on the viral surface, they are responsible for binding to host receptors (S1) and
55 membrane fusion (S2)^{1,8}. Cryo-electron microscopy on S protein has highlighted its interaction with
56 cell receptor angiotensin-converting enzyme 2 (ACE2) and the dissociation of S1 after binding to
57 the host cells. This leads S2 to a more stable state, pivotal for membrane fusion⁹⁻¹¹. Apart from
58 ACE2, also the heparan sulfate proteoglycans [HSPGs], localized on the cell surface, have been
59 recognized as the binding sites for SARS-CoV¹² and could be important also for SARS-CoV-2 in
60 the early attachment phase.

61 Lately, Wrapp and coworkers¹³, determined the first 3.5 Å resolution cryo-electron microscopy
62 [cryo-EM] structure of the SARS-CoV-2 S trimer in the prefusion conformation. Because of the
63 critical function of spike S glycoprotein in the SARS-CoV-2 infection process, the knowledge of
64 this structure, which represents a target for antibody, protein and drug mediated neutralization,

65 allowed to get atomic-level information able to guide the design and development of innovative
66 therapeutic molecules¹⁴.

67 So far, the current treatment approaches have proved inadequate and a potent antiviral drug is yet to
68 be discovered. Asymptomatic and mildly symptomatic patients remain a transmission reservoir,
69 with possible evolution to the most severe disease form, without a clear treatment indication. Innate
70 immunity should be better investigated to individuate a possible molecule with antiviral activity
71 against COVID-19, especially considering the fact that children, where innate immunity is more
72 prominent¹⁵, are less likely to suffer of severe and critical COVID-19 disease than adults^{16,17}.

73 Considering all these aspects, lactoferrin (Lf), a multifunctional glycoprotein, belonging to the
74 transferrin family, secreted by exocrine glands and neutrophils and present in all human
75 secretion^{18,19}, represents the ideal candidate to fight SARS-CoV-2²⁰.

76 Indeed, two promising *in vitro* studies, the first on SARS-CoV¹² and the second on SARS-CoV-2²¹
77 have demonstrated that Lf is able to inhibit the early phase of these two viruses and is efficient
78 against SARS-CoV-2 also in post-infection phase²¹.

79 The pleiotropic activity of Lf is mainly based on its four different functions: to chelate two ferric
80 iron per molecule, interact with anionic molecules, enter inside the nucleus and modulate iron
81 homeostasis. The ability to chelate two ferric ions per molecule is associated to the inhibition of
82 reactive oxygen species formation and the sequestration of iron, which is important for bacterial and
83 viral replication and is at the basis of the antibacterial and antiviral activity of Lf^{19,22,23}. The binding
84 to the anionic surface compounds, thanks to its cationic feature, is associated to the host protection
85 against bacterial and viral adhesion and entry¹⁹. The entrance inside host cells and the translocation
86 into the nucleus^{24,25} is related to the anti-inflammatory activity of Lf²⁶⁻²⁸ and its ability to modulate
87 iron homeostasis perturbed by viral infection and inflammation²⁹. As matter of fact, iron
88 homeostasis involves several iron proteins such as transferrin, ferroportin, hepcidin and ferritin the
89 disorders of which, induced by inflammation, lead to intracellular iron overload and viral
90 replication²⁰. Moreover, Lf seems to regulate the activation of plasminogen and control coagulation
91 cascade with a remarkable antithrombotic activity³⁰, a very frequent complication of SARS-CoV2
92³¹. In addition to all these abilities, Lf, as above reported, inhibits the early phase of SARS-CoV¹²
93 and post-infection phase of SARS-CoV-2^{12,21} probably through the binding to HSPGs or to viral
94 particles.

95 Therefore, based on this information, in order to evaluate the possibility of using Lf in the clinical
96 treatment of Covid-19, a clinical trial has been designed to validate the aforementioned assumptions
97 together with *in vitro* experimental assays and simulation.

98 In particular, we designed a prospective, interventional study in order to assess the role of oral and
99 intra-nasal liposomal Lf for COVID-19 patients with mild-to-moderate disease and COVID-19
100 asymptomatic patients, and document its efficacy in improving symptoms and clearing away the
101 virus. To study the mechanism of anti-viral activity of Lf against SARS-CoV-2, *in vitro*
102 experimental assays have been designed to validate the abovementioned postulations. The
103 hypothesis of the putative binding between spike and Lf and between viral units and host cells
104 HSPGs has been verified *in vitro* thus preliminarily demonstrating Lf antiviral activity against
105 SARS-CoV-2. Furthermore, the SARS-CoV-2 S trimer structure in prefusion conformation¹³ has
106 been used to perform a protein-protein molecular docking analysis with the aim to confirm the
107 hypothesis of a direct interaction between the Spike S glycoprotein and the Lf protein. The structure
108 of the spike glycoprotein¹³ has been completed using modelling techniques and used to predict Lf
109 interaction sites. Furthermore, the selected high-score protein-protein complex has been structurally
110 investigated using classical molecular dynamics (MD) simulation and the free energy of interaction
111 between these proteins has been evaluated through the molecular mechanic energies combined with
112 generalized Born and surface area continuum solvation (MM/GBSA) method³².

113

114 **RESULTS**

115 *Demographic data*

116 A total of 32 patients with confirmed COVID-19 infection at the real-time reverse transcription
117 polymerase chain reaction (rRT-PCR) were recruited in the COVID-19 patients' group to
118 participate in the study protocol. 22 patients had mild-to moderate symptoms and 10 patients were
119 asymptomatic. The mean age was 54.6 ± 16.9 years old. 14 patients were males and 18 females.
120 The most prevalent comorbidity was hypertension (28%) followed by cardiovascular diseases
121 (15.6%) and dementia (12.5%). 32 healthy volunteers (mean age 52.8 ± 15.5 years old.) with
122 negative rRT-PCR for SARS-CoV2 RNA were recruited in the control group to be paired to the
123 above COVID-19 group. Patients group and control group were homogeneous for age and
124 comorbidities. Clinic and demographic data of both groups are summarized in Tab.1.

125 *Primary Endpoint*

126 Real-time reverse transcription polymerase chain reaction (rRT-PCR) revealed a negative
127 conversion of SARS-COV-2 RNA of the naso-oropharyngeal swab in 10 patients (31.25%) at T1
128 and in all other patients at T2, with all patients showed a viral clearance at T2 (Fig.1)

129 *Secondary Endpoints*

130 At T0, 22 patients were symptomatic and 10 patients asymptomatic. The most frequent symptoms
131 were fatigue (50%), followed by arthralgia (37.5%) and cough (28%). At T1, 5 patients previously
132 symptomatic became asymptomatic, with a total of 17 asymptomatic and 15 symptomatic patients.
133 At T2 other 6 patients, previously symptomatic at T1, became asymptomatic with a total of 23
134 asymptomatic patients and 9 symptomatic patients. In the latter group, the most frequent symptom
135 was fatigue (21.9%). Clinical symptoms are summarized in Fig. 2 and Fig. S1(supplemental data).

136 The comparison between COVID-19 group and control group parameters at T0 showed a
137 significant difference in platelet count (p-value < 0,0001), neutrophils count (p-value= 0,04),
138 monocytes count (p-value = 0,006), D-Dimer (< 0,0001), aspartate aminotransferase (AST) (p-
139 value=0.008), ferritin (p-value < 0,0001), adrenomedullin (p-value< 0,0001) and IL-6 (p-value <
140 0,0001) (Tab. S1A, supplemental data).

141 Regarding COVID-19 group blood parameters, IL-6 value showed a significant decrease between
142 T2 and T0 (Δ_{T2-T0} -2.52 \pm 1.46, p-value 0.05). Moreover, D-dimer showed a significant decrease
143 between T2 and T0 (Δ_{T2-T0} -392.56 \pm 142.71, p-value 0.01) and ferritin presented the same
144 significant trend (Δ_{T2-T0} -90.63 \pm 48.49, p-value 0.04) (Tab. S1B, supplemental data). Regarding the
145 other values we did not achieve a statistical significance, however we noticed an improvement in
146 the platelet count (T0: 239.63 \pm 83.05; T2: 243.70 \pm 65.5; Δ_{T2-T0} 10.05 \pm 10.26) and a decrease of
147 alanine transaminase (ALT) (T0: 29.36 \pm 22.7; T2: 23.52 \pm 12.34; Δ_{T2-T0} -7.32 \pm 4.36) and AST
148 (T0:24.36 \pm 9.80;T2:22.64 \pm 8.33; Δ_{T2-T0} -2.68 \pm 2.52). Adrenomedullin remained at the same level all
149 over the analyzed period (Δ_{T2-T0} -0.01 \pm 0.03). IL-10 levels increased between T0 (8.67 \pm 3.26) and T2
150 (11.42 \pm 6.05), without showing statistical significance (Δ_{T2-T0} 2.55 \pm 2.09). TNF-alfa decreased
151 between T2 (25.97 \pm 21.74) and T0 (37.34 \pm 19.95) without showing statistical significance (Δ_{T2-T0} -
152 12.92 \pm 8.81).

153 Regarding safety assessment, 2 patients (6.2%) showed gastrointestinal complaints related to Lf
154 assumption at T2. The patients did not suspend Lf administration and the adverse event resolved
155 itself spontaneously.

156 ***Lactoferrin displays antiviral properties in in vitro models***

157 Preliminary, the doses of 100 and 500 μ g/ml of bovine Lf (bLf) in native form (7% iron saturated)
158 were assayed to detect their putative cytotoxicity by measuring cell morphology, proliferation and
159 viability of Vero E6 and Caco-2 cell monolayers after 72 h of incubation. Both 100 and 500 μ g/ml
160 of bLf do not exert any cytotoxic effect (data not shown).

161 Then, the efficacy of different concentrations of bLf in inhibiting SARS-CoV-2 infection was tested
162 on Vero E6 and Caco-2 cells according to different experimental procedures: i) control: untreated
163 SARS-CoV-2 and cells; ii) bLf pre-incubated with virus inoculum for 1 h at 37°C before cell
164 infection; iii) cells pre-incubated with bLf for 1 h at 37°C before virus infection; iv) bLf added
165 together with virus inoculum at the moment of infection step; v) virus and cells separately pre-
166 incubated with bLf for 1 h at 37°C before infection.

167 The results obtained with Vero E6 cells are shown in Figure 3A (MOI 0.1) and 3B (MOI 0.01).

168 Regarding Vero E6 cells, an inhibition of SARS-CoV-2 replication of about 1 log for multiplicity of
169 infection (MOI) 0.1 and about 2 log for MOI 0.01 on cell monolayers was observed when 100
170 µg/ml of bLf were pre-incubated for 1 h with virus before infection compared to untreated SARS-
171 CoV-2 infection ($p < 0.001$ and $p < 0.001$, respectively) (Figure 3A and 3B).

172 On the contrary, the data illustrated in Figure 3A and 3B, independently from the MOI used,
173 indicate that bLf, at this concentration, does not block SARS-CoV-2 infection when it is pre-
174 incubated with Vero E6 cells or when bLf is contemporary added to viral particles and cells at the
175 moment of infection (Figure 3A, 3B). bLf is also ineffective when it is pre-incubated for 1 h at
176 37°C separately with virus and cells before infection (Figure 3A, 3B).

177 The efficacy of 100 and 500 µg/ml of bLf against SARS-CoV-2, assayed in Caco-2 cells, is showed
178 in Figure 4 A and B (MOI 0.1) and C and D (MOI 0.01), respectively.

179 Regarding Caco-2 cells, at MOI 0.1, no significant differences were observed in all experimental
180 conditions compared to the control ones when using bLf at 100 µg/ml (Figure 4A). At MOI 0.01, an
181 inhibition of viral load in supernatants was observed at 24 hours post-infection (hpi) only when 100
182 µg/ml of bLf was pre-incubated with the viral inoculum and when the cells were pre-incubated with
183 100 µg/ml of bLf compared to the control one ($p < 0.05$) (Figure 4B). At 48 hpi, an inhibition of
184 viral load was observed only when the cells were pre-incubated with bLf ($p < 0.05$) (Figure 4B).

185 When bLf was used at a concentration of 500 µg/ml, a decrease of viral load up to 48 hpi was
186 observed when the viral inoculum was pre-incubated with bLf compared to the control group,
187 independently from the MOI used ($p < 0.05$) (Figure 4C, 4D). When the cells were pre-incubated
188 with bLf, a decrease of viral load up to 24 hpi was observed compared to the control at MOI 0.1 (p
189 < 0.001 after 6 hpi and $p < 0.05$ after 24hpi) (Figure 4C), while at MOI 0.01 the decrease of viral
190 load remained statistically significant up to 48 hpi compared to the control group ($p < 0.05$) (Figure
191 4D). When bLf was added together with SARS-CoV-2 inoculum during the adsorption step a
192 decrease of viral load up to 24 hpi was observed compared to untreated SARS-CoV-2 infection,
193 independently from the MOI used ($p < 0.001$ after 6 hpi and $p < 0.05$ after 24hpi for MOI 0.1; $p <$
194 0.05 after 6 and 24 hpi for MOI 0.01) (Figure 4C, 4D). When the cells were pre-incubated with bLf

195 and infected with SARS-CoV-2 previously pre-incubated with bLf, a decrease of viral load up to 24
196 hpi was observed for MOI 0.1 compared to untreated SARS-CoV-2 infection ($p < 0.001$ after 6 hpi
197 and $p < 0.05$ after 24hpi for MOI 0.1) (Figure 4C), while at MOI 0.01 the decrease of viral load
198 remains statistically significant up to 48 hpi compared to untreated SARS-CoV-2 infection ($p <$
199 0.05) (Figure 4D).

200 *Computational results*

201 The molecular docking simulation suggests a potential interaction of the bLf structure with the
202 spike glycoprotein CDT1 domain in the up conformation (Fig. 5A). The first three solutions
203 obtained by Frodock clustering procedure account for more than 60% of the total generated
204 complexes, which are almost completely superimposable to that shown in Fig. 5A. Starting from the
205 first Frodock solution, we performed a 30 ns long classical MD simulation in order to verify the
206 stability of the complex and check for the presence of persistent interactions between the two
207 proteins. As shown in figure S2A (supplemental data), the distance between the centers of the mass
208 of Spike and bLf, calculated as a function of time, oscillates around the value of 4.5 nm, indicating
209 a constant close contact between the two molecules. MM/GBSA analysis confirmed the high
210 affinity of the bLf for the Spike CDT1 domain (Table S2A, supplemental data), showing interaction
211 energy of -28.02 kcal/mol. In particular, MM/GBSA results highlighted that the Van der Waals
212 term mainly contribute to the binding energy (Table S2A, supplemental data).

213 A detailed analysis of the interaction network reveals the presence of 28 different interactions,
214 which persist for more than 25% of the simulation time, in agreement with the high interaction
215 energy calculated. In detail, we found 3 salt bridges, 5 hydrogen bonds and 20 residue pairs
216 involved in hydrophobic contacts (Table S3 left side, supplemental data).

217 To check if some of the Spike residues targeted by the bLf protein are involved in the binding with
218 ACE2, we have compared the average structure extracted from the simulation with the ACE2/CDT1
219 domain complex structure (PDB ID: 6LZG³³ Fig. 6). Surprisingly, only two Spike residues (Gly502
220 and Tyr505) are shared between the complexes interfaces (Table S3 left side, supplemental data), as
221 evaluated from the inspection of the superimposed structures and from the paper analysis³³. Despite
222 this, Lf holds the same position assumed by the ACE2 enzyme, i.e. above the up CDT1 domain.

223 We performed the same analysis over the evaluated human lactoferrin (hLF)-Spike complex,
224 obtaining a binding pose superimposable to that observed for the bovine protein (Fig. 5B). Besides
225 the fact that using the human protein we can still observe a persistent and close contact between the
226 two molecules (Fig. S2B, supplemental data), the analysis of the interaction network reveals the
227 presence of a larger number of interactions (45), in agreement with an higher interaction energy
228 revealed by the MM/GBSA approach (-48,25 kcal/mol, Table S3 right side, supplemental data). In

229 detail, we found 12 salt bridges, 10 hydrogen bonds and 23 residue pairs involved in hydrophobic
230 contacts (Table S2B, supplemental data), in agreement with the presence of a negative electrostatic
231 contribution term (Table S2B, supplemental data). Comparing the average structure extracted from
232 the simulation with the ACE2/CDT1 domain complex structure (PDB ID: 6LZG²¹ (Fig. S3,
233 supplemental data), we observed that also for the hLf only two residues (Thr500 and Tyr505) are
234 shared between the complexes interfaces (Table S3 right side, supplemental data).
235 These results allow us to hypothesize that, in addition to the HSPGs binding¹², both bLf and hLf
236 should be able to hinder the spike glycoprotein attachment to the ACE2 receptor, consequently
237 blocking the virus from entering into the cells.

238

239 **DISCUSSION**

240 The current treatment approaches to COVID-19 have so far proved to be inadequate, and a potent
241 antiviral drug or effective vaccine are yet to be discovered and eagerly awaited. The immediate
242 priority is to harness innate immunity in order to accelerate early antiviral immune responses.
243 Understanding the pathophysiology of COVID-19 is crucial to recognize target treatments to fight
244 the virus. Hence, in this study, we focused our attention on the anti-viral and immunomodulating
245 activity of Lf as an effective therapeutic option against COVID-19.

246 This is the first study assessing the use of Lf in the management of COVID-19 infection through *in*
247 *vivo*, *in vitro* and *in silico* evidences.

248 Several evidences based on COVID-19 clinical epidemiology indicate the role of Lf in protecting
249 against the virus also *in vivo*. Indeed, it has been reported that the incidence of COVID-19 in
250 children aged 0-10 was only 0.9% in the Chinese cases, and infants developed a less severe disease
251 form³⁴. Consecutively, some authors postulated that breast feeding or extensive use of Lf
252 containing infant formula in this population may have protected from contagion or worst disease
253 evolution³⁵.

254 Accordingly, we evaluated Lf role also *in vivo*, through a clinical trial, documenting its efficacy in
255 favoring the viral clearance and the gradual symptoms recovery in COVID-19 patients with mild-
256 to-moderate disease and in COVID-19 asymptomatic patients.

257 We focused our research on asymptomatic and mild-to-moderate COVID-19 patients, considering
258 them a transmission reservoir with possible evolution to the most severe disease form³⁶. Li et al,
259 analyzing the viral shedding dynamics in asymptomatic and mildly symptomatic patients infected
260 with SARS-CoV-2, observed a long-term viral shedding, also in the convalescent phase of the

261 disease, where specific antibody production to SARS-CoV-2 may not guarantee viral clearance
262 after hospital discharge. In their study, the median duration of viral shedding appeared to be shorter
263 in pre-symptomatic patients (11.5 days) than in asymptomatic (28 days) and mild symptomatic
264 cases (31 days)³⁷. In our study, Lf induced an early viral clearance just after 15 days from the
265 beginning of the treatment in 31% of patients, and after 30 days of treatment in the rest of our
266 patients. This early viral clearance allowed a reduction of viral shedding among our population,
267 ensuring a decrease in the risk of transmission and contagion.

268 Although there are currently rare satisfactory markers for predicting the worsening of the disease
269 until the death of patients with COVID-19, some cytokines, including IL-6, IL-10 and TNFalfa, and
270 D-Dimer levels have been described as biomarkers related to a high case fatality of SARS-CoV-2
271 infection³⁸⁻⁴¹. In our study, we identified suitable deranged blood parameters to use as treatment
272 target markers. Indeed, we found a statistically significant difference between the COVID-19 group
273 and the control group in several blood parameters, including IL-6, D-Dimer, ferritin and liver
274 function parameters. Particularly, IL-6, D-Dimer and ferritin also showed a significant decrease
275 after Lf treatment confirming them as the most suitable COVID-19 treatment target markers.

276 Particularly, IL-6 elevation is considered to be associated with higher disease severity; IL-6
277 inhibitors, such as tocilizumab, have been used to treat severe COVID-19 patients^{42,43}. The ability
278 of Lf to down-regulate pro-inflammatory cytokines, such as IL-6, has already been demonstrated
279 both in *in vitro*⁴⁴ and *in vivo*⁴⁵ models, as well as in clinical trials⁴⁶, however this is the first
280 evidence of its ability in down-regulating IL-6 also during SARS-CoV2 infection and thus the first
281 proof of its efficacy for the treatment of COVID-19.

282 We observed also a statistically significant decline in D-Dimer levels, crucial to define disease
283 prognosis, leading to a reduction in SARS-CoV-2 complications related to coagulation
284 derangement. Recently, it was shown that Lf can regulate the activation of plasminogen and control
285 coagulation cascade with a remarkable antithrombotic activity³⁰. Especially this Lf property should
286 be stressed considering that COVID-19 is a prothrombotic disease and that the severity of the
287 coagulation parameters impairment is related to a poor prognosis. Indeed, COVID-19 may represent
288 a peculiar clinicopathologic form of viral sepsis, showing a prominent prothrombotic feature instead
289 of the haemorrhagic one observed in other viral diseases. Patients affected by severe COVID-19
290 pneumonia are at higher risk of imbalance of coagulation parameters and thus treated with low
291 molecular weight heparin or unfractionated heparin at doses registered for prevention of venous
292 thromboembolism³¹. However, currently only severe patients are treated; this means that treatment
293 may begin too late.

294 Our clinical experience suggests a role of Lf in preventing the evolution of the disease, improving
295 the prognosis through its action on coagulation cascade when used since the first phases of the
296 disease. Lf can exert negative regulatory effects on cell migration via inhibition of plasminogen
297 activation and through the regulation of fibrinolysis³⁰. In addition, we observed an increased platelet
298 count after Lf treatment. Indeed, COVID-19 induces thrombocytopenia as SARS-CoV-2 seems to
299 entrap megakaryocytes and block the release of platelets. Lf rebalanced platelet count, induces
300 COVID-19 viral clearance⁴⁷.

301 Ferritin, besides reflecting the status of iron stores in healthy individuals, represents also an acute-
302 phase-protein up-regulated and elevated in both infectious and non-infectious inflammation. In
303 COVID-19, it has been reported to be relevant for assessing disease severity and patients
304 outcome^{48,49}. Iron chelators, such as Lf, have been repeatedly proposed as a potential therapeutic
305 target during infections⁵⁰ and even in COVID-19, we assessed the reduction of ferritin levels
306 during Lf administration, demonstrating its ability to chelate iron, which is pivotal for bacterial and
307 viral replication, and at the basis of its antibacterial and antiviral activity^{19,22,23}.

308 Liver function is known to be deranged in COVID-19 and a meta-analysis showed that 16% and
309 20% of patients with COVID-19 had ALT and AST levels higher than the normal range⁵¹. Liver
310 biochemistry abnormality in COVID-19 patients could be ascribed to several factors, such as direct
311 hepatocyte injury by the virus, drug-induced liver injury, hypoxic-ischemic microcirculation
312 disorder, and underlying liver diseases⁴¹. In our study, we observed that Lf therapy reduced
313 transaminases levels, decreasing the risk of liver-injury among COVID-19 patients, which is a very
314 frequent complication in SARS-CoV2 severe forms⁵². Moreover, since several treatments used to
315 treat COVID-19 severe patients, such as hydroxychloroquine, are linked to liver injuries⁵³, it could
316 be rational to use Lf together with other therapies, in order to increase viral clearance and reduce
317 adverse events of other treatments.

318 Adrenomedullin is another possible biomarker for COVID-19 prognosis, as it plays a key role in
319 reducing vascular (hyper) permeability and promoting endothelial stability and integrity following
320 severe infection⁵⁴. Indeed, recent studies have suggested that COVID-19 induced endothelial
321 dysfunction and damage could be the explanation for the development of organ dysfunction and
322 edema, resulting in impaired vascular blood flow, coagulation and leakage⁵⁵. Thus, the development
323 of endotheliitis may be a prominent, yet partly under recognized, feature of COVID-19 induced
324 severe disease. In our study, we evaluated adrenomedullin levels in COVID-19 patients after
325 receiving Lf treatment, which remained constant between T2 and T0. We explained this result

326 considering the disease severity of our population. Indeed, adrenomedullin seems to vary in most
327 severe patients⁵⁶.

328 Regarding clinical symptoms recovery, we observed a reduction in all symptoms, with the
329 exception of fatigue, which persisted in 21.9 % of patients. We explained this result considering
330 patients age and concomitant comorbidities, which could create a bias to identify COVID-19
331 symptoms.

332 Concerning Lf safety, we reported gastrointestinal complaints in 2 patients as occasional findings
333 that did not lead to treatment discontinuation. Therefore, we concluded that Lf is safe and well
334 tolerated among our study population.

335 In our analysis, we used formulations containing bLf embedded in liposomes for nasal/oral
336 administration. Indeed, the bLf at 5% of iron saturation form is best suited to obtain the maximum
337 chelating effect. Nucleic digestion, in the nasal cavities, and proteases and lipases hydrolysis, at
338 gastric and intestinal level, inactivate the protein at its first entry, cancelling or extremely reducing
339 the activity. Lf is unstable in water and is particularly sensitive to bacterial and human proteases
340 (enzymes inactivating proteins). This results in protein denaturation, poor absorption and
341 inactivation. The inclusion of Lf in preserving structures, such as liposomes, reduces gastric and
342 intestinal denaturation while maintaining its integrity and therefore its biological functionality⁵⁷⁻⁵⁹.

343 The in vitro antiviral activity of bLf against enveloped and naked DNA and RNA viruses has been
344 widely demonstrated^{12,22,23,60,61}, while few papers have been published on its in vivo efficacy against
345 viral infection⁶²⁻⁷³.

346 The ability of bLf to inhibit viral infection is generally attributed to its binding to cell surface
347 molecules and/or viral particles. BLf is able to competitively bind to heparan sulfate proteoglycans
348 (HSPGs), present on the host cell surface and identified as initial sites for enveloped viruses^{74,75},
349 thus hindering the viral adhesion and internalization^{12,76,77}. Moreover, bLf can also bind directly to
350 surface proteins of virus particles as HIV V3 loop of the gp120⁷⁸ and HCV E2 envelope proteins⁷⁹.

351 The results, presented here, by monitoring the effect of bLf on different experimental procedures
352 indicate that the antiviral activity of bLf, pre-incubated with host cells, seems to vary according to
353 MOI, different cell lines and bLf concentration. As matter of fact, the pre-incubation of Vero E6
354 monolayers with 100 µg/ml of bLf, before SARS-CoV-2 infection at MOI 0.1 and 0.01, were
355 ineffective in inhibiting virus internalization (Figure 3), differently to that observed when 100
356 µg/ml of bLf were pre-incubated with Caco-2 cells and the infection was performed at MOI 0.01
357 (Figure 4B). This antiviral activity was observed until 48 hpi.

358 The pre-incubation of 100 µg/ml of bLf with SARS-CoV-2 showed a significant antiviral activity
359 higher at 0.01 MOI compared to 0.1 MOI after infection of Vero E6 cells (Figure 3A, 3B), while a
360 significant antiviral activity assayed on Caco-2 cell lines was observed only with MOI 0.01 at 24
361 hpi (Figure 4B). In the other two experimental conditions, bLf did not show any significant antiviral
362 activity on both Vero E6 and Caco-2 cells.

363 The pre-incubation of 500 µg/ml of bLf with Caco-2 cells showed a decrease of viral load until 24
364 hpi at MOI 0.1 and up to 48 hpi at MOI 0.01. Furthermore, the pre-incubation of 500 µg/ml of bLf
365 with SARS-CoV-2 showed a significant decrease of SARS-CoV-2 RNA copies at both MOI 0.1
366 and 0.01. This antiviral activity persisted from 6 to 48 hpi (Figure 4C, 4D). In the other two
367 experimental conditions, bLf exerted a significant antiviral activity only at 6 and 24 hpi when the
368 MOI corresponded to 0.1 (Figure 4C). At MOI 0.01, a decrease of viral load up to 24 hpi was
369 observed when bLf was added together with SARS-CoV-2 inoculum during the adsorption step
370 (Figure 4D), while a decrease of viral load until 48 hpi was observed when both the cell monolayer
371 and SARS-CoV-2 were previously pre-incubated with bLf (Figure 4D).

372 Our experimental results indicate that bLf exerts its antiviral activity either by direct attachment to
373 the viral particles or by obscuring their cellular receptors. Moreover, the results obtained through
374 the molecular docking and molecular dynamics simulation approaches strongly support the
375 hypothesis of a direct recognition between the bLf and the spike S glycoprotein. The affinity
376 between their molecular surfaces, the large number of atomistic interactions detected and their
377 persistence during the simulation suggest that this recognition is very likely to occur and that bLf
378 may hinder the spike S attachment to the human ACE2 receptor, consequently blocking the virus
379 from entering into the cells.

380 Taken together these results reveal that, even if the definitive mechanism of action still has to be
381 explored, the antiviral properties of Lf are also extendable to SARS-CoV-2 virus.

382 One of the limitations of our study was the small sample size of the clinical trial. Further studies,
383 both in vitro and in vivo are needed to better deepen Lf placement against COVID-19, both as a
384 preventive, adjunctive or definitive treatment. Nevertheless, we achieved a statistical significance in
385 the crucial blood parameters related to disease evolution and we still observed an improving trend
386 in all other analyzed markers. Further studies on larger samples are needed to better evaluate the
387 role Lf in treating SARS-Cov-2.

388 Considering the risk of COVID19 relapse ⁸⁰, we also suggest additional long-term studies to
389 evaluate the maintenance of viral clearance with Lf continuous administration.

390 Finally, due to ethical reasons, we could not include placebo arms in our study and therefore we
391 could not evaluate properly the different disease evolution in treated and not-treated patients.
392 However, considering the reported natural disease course³⁷ we can state Lf induced an early RT-
393 PCR negative conversion and a fast clinical symptoms recovery.

394 This study is part of the GEFACOV2.0 research program coordinated by the Tor Vergata
395 University of Rome.

396 **MATERIALS & METHODS**

397 **Clinical trial**

398 We performed a randomized, prospective, interventional study to assess the efficacy of a liposomal
399 formulation of bovine lactoferrin (bLf) in COVID-19 patients with mild-to-moderate disease and
400 COVID-19 asymptomatic patients. Mild-to-moderate disease was defined based on less severe
401 clinical symptoms with no evidence of pneumonia and not requiring Intensive Care Unit (ICU)⁸¹
402 The primary endpoint was real-time reverse transcription polymerase chain reaction (rRT-PCR)
403 negative conversion rate of SARS-COV-2 RNA.

404 The secondary endpoints were the identification of COVID-19 deranged blood parameters and
405 therefore treatment target markers and rate of disease remission, defined as symptoms recovery and
406 blood parameters improvement. In addition, safety and tolerability of liposomal bLf for oral and
407 intra-nasal use was assessed.

408

409 *Patients (study population)*

410 Eligible patients were over 20 years old, with a confirmed COVID-19 rRT-PCR at the naso-
411 oropharyngeal swab and blood oxygen saturation (SPO2) > 93% or Horowitz index (PaO₂ / FiO₂) >
412 300mmHg. Patients did not receive any other treatment against SARS-CoV-2. Exclusion criteria
413 included pregnancy and breastfeeding, nitric oxide and nitrates assumptions, known allergy to milk
414 proteins, a medical history of bronchial hyperactivity or pre-existing respiratory diseases. ICU
415 COVID in-patients were excluded.

416 A control group of healthy volunteers, with negative rRT-PCR at the naso-oropharyngeal swab, was
417 included in the study in order to be paired to the above case-group. The "matched-pair-analysis"
418 concerned the structural and clinical characteristics of the corresponding group. Placebo or
419 liposome arms have not been included due to ethical reasons.

420 All patients gave written informed consent after receiving an extensive disclosure of the study
421 purposes and risks. To be included, patients needed to be able to understand the content of informed
422 consent and accept to sign it. The trial was approved by the Tor Vergata University Hospital Ethics

423 Committee (Code 42/20). It was registered at www.clinicalTrials.gov (NCT04475120) and reported
424 according to CONSORT guidelines (Fig. S4, supplemental data).

425

426 *Study design*

427 COVID-19 patients were consecutively enrolled from 22 April 2020 to 22 June 2020 from the
428 University Hospital of Rome Tor Vergata, from Pineta Grande Hospital of Caserta and Villa dei
429 Pini Hospital Anzio (Rome). The scheduled dose treatment of liposomal bLf for oral use was 1gr
430 per day for 30 days (10 capsules per day) in addition to the same formulation intranasally
431 administered 3 times daily.

432 BLf capsules contain 100 mg of bLf encapsulated in liposome while bLf nasal spray contains about
433 2.5 mg/ml of bLf encapsulated in liposome. bLf, contained in both products, was checked by SDS-
434 PAGE and silver nitrate staining and its purity was about 95%. The bLf iron saturation was about
435 5% as detected by optical spectroscopy at 468 nm based on an extinction coefficient of 0.54 (100%
436 iron saturation, 1% solution).

437 The control group of healthy volunteers did not receive any treatment or placebo.

438

439 *Endpoints measures*

440 rRT-PCR was performed at T0, T1(after 15 days) and T2 (after 30 days) to detect SARS-CoV-2
441 RNA in the study population.

442 All participants (COVID-19 patients and control group) underwent the following laboratory tests:
443 complete blood count and chemistry panel (liver and kidney function), iron panel, coagulation
444 profile, IL-6, IL-10, TNF α , adrenomedullin serum levels. COVID-19 patients' blood samples were
445 collected at T0 and T2; control group's blood samples were collected at T0.

446 Body temperature and evaluation of related signs and symptoms were collected at T0, T1 and T2 in
447 COVID-19 patients.

448

449 *In vitro antiviral activity of lactoferrin*

450 For *in vitro* experiments, highly purified bLf was kindly provided by Armor Proteines Industries
451 (France). BLf was checked by SDS-PAGE and silver nitrate staining. Its purity was about 98% and
452 its concentration was confirmed by UV spectroscopy according to an extinction coefficient of 15.1
453 (280 nm, 1% solution). The bLf iron saturation was about 7% as detected by optical spectroscopy at
454 468 nm based on an extinction coefficient of 0.54 (100% iron saturation, 1% solution). LPS
455 contamination of bLf, estimated by Limulus Amebocyte assay (Pyrochrome kit, PBI International,
456 Italy), was equal to 0.6 ± 0.05 ng/mg of bLf. Before each *in vitro* assays, bLf solution was sterilized

457 by filtration using 0.2 µm Millex HV at low protein retention (Millipore Corp., Bedford, MA,
458 USA).

459

460 ***Cell culture and virus***

461 The African green monkey kidney-derived Vero E6 and human colon carcinoma-derived Caco-2
462 cells were provided by American Type Culture Collection (ATCC). Cells were grown in high-
463 glucose Dulbecco's modified Eagle's medium (DMEM) (Euroclone, Milan, Italy) supplemented
464 with 10% fetal bovine serum (FBS) (Euroclone, Milan, Italy) at 37°C in humidified incubators with
465 5% CO₂. SARS-CoV-2 strain was isolated from nasopharyngeal specimen taken from a patient with
466 laboratory confirmed COVID-19 and was propagated in Vero E6 cells. Viral titres were determined
467 by 50% tissue culture infectious dose (TCID₅₀) assays in Vero E6 (Spearman-Kärber method) by
468 microscopic scoring. All experiments were performed by infecting Vero E6 and Caco-2 cells with
469 SARS-CoV-2 strain at the Department of Molecular Medicine, University of Padua, under
470 Biosafety Level 3 (BSL3) protocols, in compliance with laboratory containment procedures
471 approved by the University of Padua.

472 ***Cytotoxicity assay***

473 Cytotoxicity was evaluated by incubating 100 and 500 µg of bLf - the concentrations used for
474 invitro experiments - in DMEM containing 10% of FBS for 72 h at 37°C with Vero E6 and Caco-2
475 cells in 96-well microtiter plates. Cell proliferation and viability were assessed by MTT assay
476 (Merck, Italy). Tetrazolium salts used for quantifying viable cells were cleaved to form a formazan
477 dye, which was evaluated by spectrophotometric absorbance at 600 nm.

478 ***Infection assay***

479 For infection assay, Vero E6 cells were seeded in 24-well tissue culture plates at a concentration of
480 1×10^5 cells/well for 24h at 37°C in humidified incubators with 5% CO₂, while Caco-2 cells were
481 seeded at a concentration of 2×10^5 cells/well for 48h at 37°C in humidified incubators with 5%
482 CO₂. 100 µg of bLf for Vero E6 infection assay, while 100 and 500 µg of bLf were used for Caco-2
483 infection assay. In order to investigate the putative interaction of bLf with viral particles and/or host
484 cells, the following different experimental approaches were performed. To evaluate if bLf can
485 interfere with the viral infectivity rate by binding viral surface components, SARS-CoV-2 at
486 multiplicity of infection (MOI) of 0.1 and 0.01 was pre-incubated with bLf for 1h at 37°C in
487 humidified incubators with 5% CO₂. The cells were then infected with these suspensions for 1h at
488 37°C in humidified incubators with 5% CO₂. In order to evaluate if bLf interferes with the viral

489 attachment to host cells, the cells were pre-incubated in culture medium without FBS with bLf for
490 1h at 37°C in humidified incubators with 5% CO₂. The cells were then washed with phosphate
491 buffered saline (PBS) and infected with SARS-CoV-2 at MOI of 0.1 and 0.01 for 1h at 37°C in
492 humidified incubators with 5% CO₂. To assess if bLf can interfere with both viral and host cell
493 components, bLf was added together with SARS-CoV-2 at MOI of 0.1 and 0.01 to cell monolayer
494 for 1h at 37°C in humidified incubators with 5% CO₂. In addition, the pre-incubation of SARS-
495 CoV-2 with bLf for 1h at 37°C was used to infect cell monolayer previously pre-treated with bLf
496 for 1 h at 37°C.

497 Regarding Vero E6 cells, after each experimental approach, the cells were washed with PBS,
498 overlaid with DMEM containing 0.75% of carboxymethylcellulose and 2% of FBS and incubated
499 for 48h at 37°C in humidified incubators with 5% CO₂. After 48h, the cells were washed, fixed with
500 5% of formaldehyde for 10 min at room temperature and stained with crystal violet at 1% for 5 min.
501 The number of plaques was determined after extensive washing.

502 The other infection experiments were carried out with Caco-2 cells. Substantial cell death was not
503 detected up to 7 days on Caco-2 cells after SARS-CoV-2 infection at MOI 0.1⁸². In this respect,
504 after each experimental procedure, the cell monolayers were replaced with DMEM with 2% of FBS
505 and after 6, 24 and 48 hpi the supernatant samples were collected for RNA extraction and
506 quantitative real-time reverse transcription (RT)-PCR analysis of viral particles. Briefly, we lysed
507 200 µl of viral supernatant in an equal volume of NUCLISENS easyMAG lysis buffer (Biomérieux,
508 France). Detection of SARS-CoV-2 RNA was performed by an in-house real-time RT-PCR
509 method, which was developed according the protocol and the primers and probes designed by
510 Corman et al.⁸³ that targeted the genes encoding envelope (E) (E_Sarbeco_F, E_Sarbeco_R and
511 E_Sarbeco_P1) of SARS-CoV-2. Quantitative RT-PCR assays were performed in a final volume of
512 25 µl, containing 5 µl of purified nucleic acids, using One Step Real Time kit (Thermo Fisher
513 Scientific) and run on ABI 7900HT Fast Sequence Detection Systems (Thermo Fisher Scientific).
514 Cycle threshold (Ct) data from RT-PCR assays were collected for E genes. Genome equivalent
515 copies per ml were inferred according to linear regression performed on calibration standard curves.

516 ***Protein-protein docking methods***

517 The structure of the SARS-CoV-2 spike glycoprotein in prefusion conformation was extracted from
518 a clustering procedure carried out as indicated in a previously published paper¹⁴. The three-
519 dimensional structure of the diferric forms of bLf and hLf, refined at 2.8 Å and 2.2 resolution
520 respectively, were downloaded from the PDB Database (PDB IDs: 1BFL,¹² and 1B0L,⁸⁴). The
521 protein-protein docking analysis between the modelled SARS-CoV-2 spike glycoprotein¹ and the Lf
522 structures was carried out using the Frodock docking algorithm⁸⁵. Frodock's approach combines

523 the projection of the interaction terms into 3D grid-based potentials and the binding energy upon
524 complex formation, which is approximated as a correlation function composed of van der Waals,
525 electrostatics and desolvation potential terms. The interaction-energy minima are identified through
526 a fast and exhaustive rotational docking search combined with a simple translational scanning⁸⁶.
527 Both docking procedures were performed using Frodock's (<http://frodock.chaconlab.org/>) web-
528 server.

529

530 ***Molecular dynamics***

531 Topology and coordinate files of the input structures were generated using the tLeap module of the
532 AmberTools 19 package⁸⁷. The spike glycoprotein and Lf were parametrized using the ff19SB
533 force field, and were inserted into a rectangular box of TIP3P water molecules, with a minimum
534 distance of 12.0 Å from the box sides, and after neutralizing the solution with 0.15 mol/L of NaCl
535 ions. To remove unfavourable interactions, all structures underwent four minimization cycles, each
536 composed by 500 steps of steepest descent minimization followed by 1500 steps of conjugated
537 gradient minimization. An initial restraint of 20.0 kcal • mol⁻¹ • Å⁻² was imposed on protein atoms
538 and subsequently reduced and removed in the last minimization cycle. Systems were gradually
539 heated from 0 to 300 K in a NVT ensemble over a period of 2.0 ns using the Langevin thermostat,
540 imposing a starting restraint of 0.5 kcal • mol⁻¹ • Å⁻² on each atom, which was decreased every
541 500 ps in order to slowly relax the system. The systems were simulated in an isobaric-isothermal
542 (NPT) ensemble for 2.0 ns, imposing a pressure of 1.0 atm using the Langevin barostat and fixing
543 the temperature at 300 K. Covalent bonds involving hydrogen atoms were constrained using the
544 SHAKE algorithm⁸⁸. A production run of 30 ns was performed for with a timestep of 2.0 fs, using
545 the NAMD 2.13 MD package⁸⁹. The PME method was used to calculate long-range interactions,
546 while a cut-off of 9.0 Å was set for short-range interactions. System coordinates were saved every
547 1000 steps.

548

549 ***Trajectory analysis***

550 Distance analysis was performed using the distance module of the GROMACS 2019 analysis tools
551⁹⁰, while hydrogen bond persistence was evaluated using the hbonds module coupled to in-house
552 written codes. The hydrophobic contacts were identified using the *contact_map* and
553 *contact_frequency* routines of the mdtraj Python library⁹¹. Generalized Born and surface area
554 continuum solvation (MM/GBSA) analysis were performed over the last 15 ns of the trajectories,
555 using the MMPBSA.py.MPI program implemented in the AMBER16 software⁹² on 2 nodes of the

556 ENEA HPC cluster CRESCO6⁹³. Pictures of the Spike-Laf and Spike RBD-ACE2 complexes were
557 generated using the UCSF Chimera program⁹⁴.

558

559 ***Statistical analysis***

560 Descriptive and inferential statistical analyses were performed. The Kolmogorov–Smirnov test was
561 used to check the normal distribution of blood parameters.

562 Blood parameters obtained at T0 in COVID-19 group and control group were compared using t-test.

563 Data were then analyzed with a significant two-tailed p-value ≤ 0.05 .

564 All parameters obtained at T0 and T2 in COVID-19 group were then compared using paired t-test.

565 In addition, the mean change between T0 and T2 was also assessed using paired t-test. Normally
566 distributed data were then analyzed with a significant p-value ≤ 0.05 .

567 For what concerns in vitro experiments, the number of plaque forming units (pfu)/ml of SARS-
568 CoV-2 on Vero E6 cells and the number of SARS-CoV-2 RNA copies/ml on Caco-2 cells in each
569 experimental approach was compared with the control ones (untreated SARS-CoV-2 and cells) at
570 the same time point in order to assess the statistically significant differences by using unpaired
571 student's *t* tests. Results are expressed as the mean values \pm standard deviation (SD) of three
572 independent experiments. In each case, a *p* value ≤ 0.05 was considered statistically significant.

573

574 **Acknowledgements**

575 We thank Prof. Denis Mariano for English language editing.

576 We thank Technology Dedicated To Care (TDC) and mainly Dr. Biagio Biancardi, Dr. Martina
577 Biancardi, Dr. Luigi Biancardi, for their expertise. In addition, we thank Dr. Alessandra Nistri and
578 Prof. Maria Grazia Marciani and Prof. Giuseppe Novelli.

579 We thank Dr. Giancarlo Mennella of Egamid for technical support.

580 The computing resources and the related technical support were provided by CRESCO/ENEAGRID
581 High Performance Computing infrastructure. CRESCO/ENEAGRID High Performance Computing
582 infrastructure is funded by ENEA, the Italian National Agency for New Technologies, Energy and
583 Sustainable Economic Development and by Italian and European research programmes, see
584 <http://www.cresco.enea.it/english> for information.

585 **Author Contributions:** Conceptualization, EC, PV, LB, MF, AM; Formal analysis, CC;
586 Investigation, EC, TC, LR, MPC, FI, AR, CDV, EF, SL, MM, MC, MN, AT, II, LC, AM, SB, NM,

587 SS, FR, PLB; Writing- original draft, CL, EC, LR, LB, PV, MF; Writing-review & editing, EC, LB,
588 PV

589 **Declaration of Interests:** none

590

591 **FIGURE LEGENDS**

592 **Tab.1** Demographic and clinic data

593 **Figure 1** SARS-COV-2 RNA rRT-PCR trend

594 **Figure 2** Clinical symptoms recovery trend

595 **Figure 3** Plaque forming units (pfu)/ml of SARS-CoV-2 observed in Vero E6 cells infected at
596 multiplicity of infection (MOI) of 0.1 (**A**) and 0.01 (**B**) in the presence or absence of 100 µg/ml of
597 bovine lactoferrin (bLf) according to the following experimental procedures: i) control: untreated
598 SARS-CoV-2 and Vero E6 cells; ii) bLf pre-incubated with SARS-CoV-2 inoculum for 1h at 37°C
599 before cell infection iii) cells pre-incubated with bLf for 1 h at 37°C before SARS-CoV-2 infection;
600 iv) bLf added together with SARS-CoV-2 inoculum during the adsorption step; v) virus and cells
601 separately pre-incubated with bLf for 1 h at 37°C before infection. Data represent the mean values
602 of three independent experiments. Error bars: standard error of the mean. Statistical significance is
603 indicated as follows: **: $p < 0.001$, ***: $p < 0.0001$ (Unpaired student's t test).

604 **Figure 4.** RNA copies/ml of SARS-CoV-2 observed in supernatants of Caco-2 cells infected at
605 multiplicity of infection (MOI) of 0.1 (**A,C**) and 0.01 (**B,D**) in the presence or absence of 100 µg/ml
606 (**A,B**) and 500 µg/ml (**C,D**) of bovine lactoferrin (bLf) according to the following experimental
607 procedures: i) control: untreated SARS-CoV-2 and Caco-2 cells; ii) bLf pre-incubated with SARS-
608 CoV-2 inoculum for 1h at 37°C before cell infection iii) cells pre-incubated with bLf for 1 h at
609 37°C before SARS-CoV-2 infection; iv) bLf added together with SARS-CoV-2 inoculum during
610 the adsorption step; v) virus and cells separately pre-incubated with bLf for 1 h at 37°C before
611 infection. Viral supernatant samples were harvested at 6, 24 and 48 hours post infection (hpi). Viral
612 loads were ascertained with quantitative RT-PCR. Data represent the mean values of three
613 independent experiments. Error bars: standard error of the mean. Statistical significance is indicated
614 as follows: *: $p < 0.05$, **: $p < 0.001$ (Unpaired student's t test).

615

616 **Figure 5:** Spacefill representations of the best molecular complex obtained with Frodock between
617 the bovine (A) and human (B) lactoferrin with the Spike glycoprotein. The red, blue and green
618 colours represent the Spike glycoprotein chains, while the yellow depicts the lactoferrin molecules.

619 **Figure 6:** Comparison of the Frodock best complex and of the ACE2-Spike glycoprotein (PDB ID:
620 6LZG). The red, blue and green solid surfaces represent the three different chains composing the

621 Spike glycoprotein. The black ribbons highlight the CTD1 domain in the up conformation. The
622 magenta and yellow ribbons represent the ACE2 (A) and the bovine lactoferrin (B), respectively,
623 surrounded by a transparent molecular surface representation, in order to point out the positions
624 occupied in the space by the different structures.

625 REFERENCES

- 626 1. Lu, R. *et al.* Genomic characterisation and epidemiology of 2019 novel coronavirus:
627 implications for virus origins and receptor binding. *Lancet* **395**, 565–574 (2020).
- 628 2. Tian, X. *et al.* Potent binding of 2019 novel coronavirus spike protein by a SARS
629 coronavirus-specific human monoclonal antibody. *Emerg Microbes Infect* **9**, 382–385 (2020).
- 630 3. Su, S. *et al.* Epidemiology, Genetic Recombination, and Pathogenesis of Coronaviruses.
631 *Trends Microbiol.* **24**, 490–502 (2016).
- 632 4. Menachery, V. D., Debbink, K. & Baric, R. S. Coronavirus non-structural protein 16:
633 evasion, attenuation, and possible treatments. *Virus Res.* **194**, 191–199 (2014).
- 634 5. Forni, D., Cagliani, R., Clerici, M. & Sironi, M. Molecular Evolution of Human Coronavirus
635 Genomes. *Trends Microbiol.* **25**, 35–48 (2017).
- 636 6. Lan, J. *et al.* Structure of the SARS-CoV-2 spike receptor-binding domain bound to the
637 ACE2 receptor. *Nature* **581**, 215–220 (2020).
- 638 7. Cui, J., Li, F. & Shi, Z.-L. Origin and evolution of pathogenic coronaviruses. *Nat. Rev.*
639 *Microbiol.* **17**, 181–192 (2019).
- 640 8. Li, F. Structure, Function, and Evolution of Coronavirus Spike Proteins. *Annu Rev Virol* **3**,
641 237–261 (2016).
- 642 9. Gui, M. *et al.* Cryo-electron microscopy structures of the SARS-CoV spike glycoprotein
643 reveal a prerequisite conformational state for receptor binding. *Cell Res.* **27**, 119–129 (2017).
- 644 10. Kirchdoerfer, R. N. *et al.* Stabilized coronavirus spikes are resistant to conformational
645 changes induced by receptor recognition or proteolysis. *Sci Rep* **8**, 15701 (2018).
- 646 11. Yuan, Y. *et al.* Cryo-EM structures of MERS-CoV and SARS-CoV spike glycoproteins
647 reveal the dynamic receptor binding domains. *Nat Commun* **8**, 15092 (2017).
- 648 12. Lang, J. *et al.* Inhibition of SARS pseudovirus cell entry by lactoferrin binding to heparan
649 sulfate proteoglycans. *PLoS ONE* **6**, e23710 (2011).
- 650 13. Wrapp, D. *et al.* Cryo-EM Structure of the 2019-nCoV Spike in the Prefusion Conformation.
651 *bioRxiv* (2020) doi:10.1101/2020.02.11.944462.
- 652 14. Romeo, A., Iacovelli, F. & Falconi, M. Targeting the SARS-CoV-2 spike glycoprotein
653 prefusion conformation: virtual screening and molecular dynamics simulations applied to the
654 identification of potential fusion inhibitors. *Virus Res* **286**, 198068–198068 (2020).
- 655 15. Chang, R, Sun, WZ & Ng, TB. Lactoferrin as potential preventative and treatment for
656 COVID-19. *Authorea* (2020).
- 657 16. Carsetti, R. *et al.* The immune system of children: the key to understanding SARS-CoV-2
658 susceptibility? *Lancet Child Adolesc Health* **4**, 414–416 (2020).
- 659 17. Ludvigsson, J. F. Systematic review of COVID-19 in children shows milder cases and a
660 better prognosis than adults. *Acta Paediatr.* **109**, 1088–1095 (2020).
- 661 18. Rosa, L., Cutone, A., Lepanto, M. S., Paesano, R. & Valenti, P. Lactoferrin: A Natural

- 662 Glycoprotein Involved in Iron and Inflammatory Homeostasis. *Int J Mol Sci* **18**, (2017).
- 663 19. Valenti, P. & Antonini, G. Lactoferrin: an important host defence against microbial and viral
664 attack. *Cell. Mol. Life Sci.* **62**, 2576–2587 (2005).
- 665 20. Campione, E. *et al.* Lactoferrin as Protective Natural Barrier of Respiratory and Intestinal
666 Mucosa against Coronavirus Infection and Inflammation. *Int J Mol Sci* **21**, (2020).
- 667 21. Mirabelli, C. *et al.* Morphological Cell Profiling of SARS-CoV-2 Infection Identifies Drug
668 Repurposing Candidates for COVID-19. *bioRxiv* (2020) doi:10.1101/2020.05.27.117184.
- 669 22. Berlutti, F. *et al.* Antiviral properties of lactoferrin--a natural immunity molecule. *Molecules*
670 **16**, 6992–7018 (2011).
- 671 23. Wakabayashi, H., Oda, H., Yamauchi, K. & Abe, F. Lactoferrin for prevention of common
672 viral infections. *J. Infect. Chemother.* **20**, 666–671 (2014).
- 673 24. Ashida, K., Sasaki, H., Suzuki, Y. A. & Lönnerdal, B. Cellular internalization of lactoferrin
674 in intestinal epithelial cells. *Biometals* **17**, 311–315 (2004).
- 675 25. Lepanto, M. S., Rosa, L., Paesano, R., Valenti, P. & Cutone, A. Lactoferrin in Aseptic and
676 Septic Inflammation. *Molecules* **24**, (2019).
- 677 26. Kruzel, M. L., Zimecki, M. & Actor, J. K. Lactoferrin in a Context of Inflammation-Induced
678 Pathology. *Front Immunol* **8**, 1438 (2017).
- 679 27. Liao, Y., Jiang, R. & Lönnerdal, B. Biochemical and molecular impacts of lactoferrin on
680 small intestinal growth and development during early life. *Biochem. Cell Biol.* **90**, 476–484 (2012).
- 681 28. Suzuki, Y. A., Wong, H., Ashida, K.-Y., Schryvers, A. B. & Lönnerdal, B. The N1 domain
682 of human lactoferrin is required for internalization by caco-2 cells and targeting to the nucleus.
683 *Biochemistry* **47**, 10915–10920 (2008).
- 684 29. Mancinelli, R. *et al.* Viral Hepatitis and Iron Dysregulation: Molecular Pathways and the
685 Role of Lactoferrin. *Molecules* **25**, (2020).
- 686 30. Zwirzitz, A. *et al.* Lactoferrin is a natural inhibitor of plasminogen activation. *J. Biol. Chem.*
687 **293**, 8600–8613 (2018).
- 688 31. Marietta, M., Coluccio, V. & Luppi, M. COVID-19, coagulopathy and venous
689 thromboembolism: more questions than answers. *Intern Emerg Med* (2020) doi:10.1007/s11739-
690 020-02432-x.
- 691 32. Genheden, S. & Ryde, U. The MM/PBSA and MM/GBSA methods to estimate ligand-
692 binding affinities. *Expert Opin Drug Discov* **10**, 449–461 (2015).
- 693 33. Wang, Q. *et al.* Structural and Functional Basis of SARS-CoV-2 Entry by Using Human
694 ACE2. *Cell* **181**, 894-904.e9 (2020).
- 695 34. Hong, H., Wang, Y., Chung, H.-T. & Chen, C.-J. Clinical characteristics of novel
696 coronavirus disease 2019 (COVID-19) in newborns, infants and children. *Pediatr Neonatol* **61**,
697 131–132 (2020).
- 698 35. Chang, R., Ng, T. B. & Sun, W.-Z. Lactoferrin as potential preventative and treatment for
699 COVID-19. *Int. J. Antimicrob. Agents* 106118 (2020) doi:10.1016/j.ijantimicag.2020.106118.

- 700 36. Jiang, X.-L. *et al.* Transmission Potential of Asymptomatic and Paucisymptomatic Severe
701 Acute Respiratory Syndrome Coronavirus 2 Infections: A 3-Family Cluster Study in China. *J.*
702 *Infect. Dis.* **221**, 1948–1952 (2020).
- 703 37. Li, W. *et al.* Viral shedding dynamics in asymptomatic and mildly symptomatic patients
704 infected with SARS-CoV-2. *Clin. Microbiol. Infect.* (2020) doi:10.1016/j.cmi.2020.07.008.
- 705 38. Aziz, M., Fatima, R. & Assaly, R. Elevated interleukin-6 and severe COVID-19: A meta-
706 analysis. *J. Med. Virol.* (2020) doi:10.1002/jmv.25948.
- 707 39. Li, L.-Q. *et al.* COVID-19 patients' clinical characteristics, discharge rate, and fatality rate
708 of meta-analysis. *J. Med. Virol.* **92**, 577–583 (2020).
- 709 40. Tang, N., Li, D., Wang, X. & Sun, Z. Abnormal coagulation parameters are associated with
710 poor prognosis in patients with novel coronavirus pneumonia. *J. Thromb. Haemost.* **18**, 844–847
711 (2020).
- 712 41. Xu, Z. *et al.* Pathological findings of COVID-19 associated with acute respiratory distress
713 syndrome. *Lancet Respir Med* **8**, 420–422 (2020).
- 714 42. Cortegiani, A. *et al.* Rationale and evidence on the use of tocilizumab in COVID-19: a
715 systematic review. *Pulmonology* (2020) doi:10.1016/j.pulmoe.2020.07.003.
- 716 43. Maeda, T., Obata, R., Do, D. R. & Kuno, T. The Association of Interleukin-6 value,
717 Interleukin inhibitors and Outcomes of Patients with COVID-19 in New York City. *Journal of*
718 *Medical Virology* **n/a**,.
- 719 44. Cutone, A. *et al.* Lactoferrin Efficiently Counteracts the Inflammation-Induced Changes of
720 the Iron Homeostasis System in Macrophages. *Front Immunol* **8**, 705 (2017).
- 721 45. Valenti, P. *et al.* Aerosolized bovine lactoferrin reduces neutrophils and pro-inflammatory
722 cytokines in mouse models of *Pseudomonas aeruginosa* lung infections. *Biochem. Cell Biol.* **95**, 41–
723 47 (2017).
- 724 46. Lepanto, M. S. *et al.* Efficacy of Lactoferrin Oral Administration in the Treatment of
725 Anemia and Anemia of Inflammation in Pregnant and Non-pregnant Women: An Interventional
726 Study. *Front Immunol* **9**, 2123 (2018).
- 727 47. Thachil, J. What do monitoring platelet counts in COVID-19 teach us? *J. Thromb. Haemost.*
728 (2020) doi:10.1111/jth.14879.
- 729 48. Bolondi, G. *et al.* Iron metabolism and lymphocyte characterisation during Covid-19
730 infection in ICU patients: an observational cohort study. *World J Emerg Surg* **15**, (2020).
- 731 49. Kappert, K., Jahić, A. & Tauber, R. Assessment of serum ferritin as a biomarker in COVID-
732 19: bystander or participant? Insights by comparison with other infectious and non-infectious
733 diseases. *Biomarkers* **0**, 1–36 (2020).
- 734 50. Dalamaga, M., Karampela, I. & Mantzoros, C. S. Commentary: Could iron chelators prove
735 to be useful as an adjunct to COVID-19 Treatment Regimens? *Metab. Clin. Exp.* **108**, 154260
736 (2020).
- 737 51. Deng, X. *et al.* Blood biochemical characteristics of patients with coronavirus disease 2019
738 (COVID-19): a systemic review and meta-analysis. *Clin. Chem. Lab. Med.* **58**, 1172–1181 (2020).

- 739 52. Wang, Q. *et al.* Pattern of liver injury in adult patients with COVID-19: a retrospective
740 analysis of 105 patients. *Mil Med Res* **7**, 28 (2020).
- 741 53. Kelly, M. *et al.* Clinical outcomes and adverse events in patients hospitalised with COVID -
742 19, treated with off- label hydroxychloroquine and azithromycin. *Br J Clin Pharmacol* (2020)
743 doi:10.1111/bcp.14482.
- 744 54. Wilson, D. C. *et al.* Adrenomedullin in COVID-19 induced endotheliitis. *Crit Care* **24**,
745 (2020).
- 746 55. Varga, Z. *et al.* Endothelial cell infection and endotheliitis in COVID-19. *Lancet* **395**, 1417–
747 1418 (2020).
- 748 56. Christ-Crain, M. *et al.* Pro-adrenomedullin to predict severity and outcome in community-
749 acquired pneumonia [ISRCTN04176397]. *Crit Care* **10**, R96 (2006).
- 750 57. Kato, Y., Hosokawa, T., Hayakawa, E. & Ito, K. Influence of liposomes on tryptic digestion
751 of insulin. II. *Biol. Pharm. Bull.* **16**, 740–744 (1993).
- 752 58. Liu, W., Wei, F., Ye, A., Tian, M. & Han, J. Kinetic stability and membrane structure of
753 liposomes during in vitro infant intestinal digestion: Effect of cholesterol and lactoferrin. *Food*
754 *Chem* **230**, 6–13 (2017).
- 755 59. Meshulam, D. & Lesmes, U. Responsiveness of emulsions stabilized by lactoferrin nano-
756 particles to simulated intestinal conditions. *Food Funct* **5**, 65–73 (2014).
- 757 60. Ng, T. B. *et al.* Antiviral activities of whey proteins. *Appl. Microbiol. Biotechnol.* **99**, 6997–
758 7008 (2015).
- 759 61. van der Strate, B. W., Beljaars, L., Molema, G., Harmsen, M. C. & Meijer, D. K. Antiviral
760 activities of lactoferrin. *Antiviral Res.* **52**, 225–239 (2001).
- 761 62. Chen, H.-L. *et al.* Recombinant porcine lactoferrin expressed in the milk of transgenic mice
762 protects neonatal mice from a lethal challenge with enterovirus type 71. *Vaccine* **26**, 891–898
763 (2008).
- 764 63. Egashira, M., Takayanagi, T., Moriuchi, M. & Moriuchi, H. Does daily intake of bovine
765 lactoferrin-containing products ameliorate rotaviral gastroenteritis? *Acta Paediatr.* **96**, 1242–1244
766 (2007).
- 767 64. Hirashima, N. *et al.* A randomized controlled trial of consensus interferon with or without
768 lactoferrin for chronic hepatitis C patients with genotype 1b and high viral load. *Hepatol. Res.* **29**,
769 9–12 (2004).
- 770 65. Ishibashi, Y. *et al.* Randomized placebo-controlled trial of interferon alpha-2b plus ribavirin
771 with and without lactoferrin for chronic hepatitis C. *Hepatol. Res.* **32**, 218–223 (2005).
- 772 66. L, G. *et al.* Lack of effect of bovine lactoferrin in respiratory syncytial virus replication and
773 clinical disease severity in the mouse model. *Antiviral research* vol. 99
774 <https://pubmed.ncbi.nlm.nih.gov/23735300/> (2013).
- 775 67. Lu, L. *et al.* Protective influence of lactoferrin on mice infected with the polycythemia-
776 inducing strain of Friend virus complex. *Cancer Res.* **47**, 4184–4188 (1987).
- 777 68. Okada, S. *et al.* Dose-response trial of lactoferrin in patients with chronic hepatitis C. *Jpn. J.*

- 778 *Cancer Res.* **93**, 1063–1069 (2002).
- 779 69. Shin, K. *et al.* Effects of orally administered bovine lactoferrin and lactoperoxidase on
780 influenza virus infection in mice. *J. Med. Microbiol.* **54**, 717–723 (2005).
- 781 70. Tanaka, K. *et al.* Lactoferrin inhibits hepatitis C virus viremia in patients with chronic
782 hepatitis C: a pilot study. *Jpn. J. Cancer Res.* **90**, 367–371 (1999).
- 783 71. Ueno, H. *et al.* Randomized, double-blind, placebo-controlled trial of bovine lactoferrin in
784 patients with chronic hepatitis C. *Cancer Sci.* **97**, 1105–1110 (2006).
- 785 72. Vitetta, L. *et al.* The clinical efficacy of a bovine lactoferrin/whey protein Ig-rich fraction
786 (Lf/IgF) for the common cold: a double blind randomized study. *Complement Ther Med* **21**, 164–
787 171 (2013).
- 788 73. Yen, M.-H., Chiu, C.-H., Huang, Y.-C. & Lin, T.-Y. Effects of lactoferrin-containing
789 formula in the prevention of enterovirus and rotavirus infection and impact on serum cytokine
790 levels: a randomized trial. *Chang Gung Med J* **34**, 395–402 (2011).
- 791 74. Sapp, M. & Bienkowska-Haba, M. Viral entry mechanisms: human papillomavirus and a
792 long journey from extracellular matrix to the nucleus. *FEBS J* **276**, 7206–7216 (2009).
- 793 75. Spear, P. G. Herpes simplex virus: receptors and ligands for cell entry. *Cell. Microbiol.* **6**,
794 401–410 (2004).
- 795 76. Chien, Y.-J., Chen, W.-J., Hsu, W.-L. & Chiou, S.-S. Bovine lactoferrin inhibits Japanese
796 encephalitis virus by binding to heparan sulfate and receptor for low density lipoprotein. *Virology*
797 **379**, 143–151 (2008).
- 798 77. Marchetti, M., Trybala, E., Superti, F., Johansson, M. & Bergström, T. Inhibition of herpes
799 simplex virus infection by lactoferrin is dependent on interference with the virus binding to
800 glycosaminoglycans. *Virology* **318**, 405–413 (2004).
- 801 78. Swart, P. j. *et al.* Antiviral Effects of Milk Proteins: Acylation Results in Polyanionic
802 Compounds with Potent Activity against Human Immunodeficiency Virus Types 1 and 2 in Vitro.
803 *AIDS Research and Human Retroviruses* **12**, 769–775 (1996).
- 804 79. Nozaki, A. *et al.* Identification of a lactoferrin-derived peptide possessing binding activity to
805 hepatitis C virus E2 envelope protein. *J. Biol. Chem.* **278**, 10162–10173 (2003).
- 806 80. Prévost, J. *et al.* Cross-sectional evaluation of humoral responses against SARS-CoV-2
807 Spike. *bioRxiv* (2020) doi:10.1101/2020.06.08.140244.
- 808 81. Xu, Y.-H. *et al.* Clinical and computed tomographic imaging features of novel coronavirus
809 pneumonia caused by SARS-CoV-2. *Journal of Infection* **80**, 394–400 (2020).
- 810 82. Chu, H. *et al.* Comparative tropism, replication kinetics, and cell damage profiling of SARS-
811 CoV-2 and SARS-CoV with implications for clinical manifestations, transmissibility, and
812 laboratory studies of COVID-19: an observational study. *The Lancet Microbe* **1**, e14–e23 (2020).
- 813 83. Corman, V. M. *et al.* Detection of 2019 novel coronavirus (2019-nCoV) by real-time RT-
814 PCR. *Euro Surveill.* **25**, (2020).
- 815 84. Sun, X.-L., Baker, H. M., Shewry, S. C., Jameson, G. B. & Baker, E. N. Structure of
816 recombinant human lactoferrin expressed in *Aspergillus awamori*. *Acta Crystallographica Section*

- 817 *D* **55**, 403–407 (1999).
- 818 85. Ramírez-Aportela, E., López-Blanco, J. R. & Chacón, P. FRODOCK 2.0: fast protein-
819 protein docking server. *Bioinformatics* **32**, 2386–2388 (2016).
- 820 86. Garzon, J. I. *et al.* FRODOCK: a new approach for fast rotational protein-protein docking.
821 *Bioinformatics* **25**, 2544–2551 (2009).
- 822 87. Salomon Ferrer, R., Case, D. A. & Walker, R. C. An overview of the Amber biomolecular
823 simulation package. *WIREs Computational Molecular Science* **3**, 198–210 (2013).
- 824 88. Ryckaert, J.-P., Ciccotti, G. & Berendsen, H. J. C. Numerical integration of the cartesian
825 equations of motion of a system with constraints: molecular dynamics of n-alkanes. *Journal of*
826 *Computational Physics* **23**, 327–341 (1977).
- 827 89. Phillips, J. C. *et al.* Scalable molecular dynamics with NAMD. *J Comput Chem* **26**, 1781–
828 1802 (2005).
- 829 90. Abraham, M. J. *et al.* GROMACS: High performance molecular simulations through multi-
830 level parallelism from laptops to supercomputers. *SoftwareX* **1–2**, 19–25 (2015).
- 831 91. McGibbon, R. T. *et al.* MDTraj: A Modern Open Library for the Analysis of Molecular
832 Dynamics Trajectories. *Biophys. J.* **109**, 1528–1532 (2015).
- 833 92. Case, D. *et al.* *Amber 2016*. (Univ. California, 2016).
- 834 93. Ponti, G. *et al.* The role of medium size facilities in the HPC ecosystem: the case of the new
835 CRESCO4 cluster integrated in the ENEAGRID infrastructure. in *2014 International Conference*
836 *on High Performance Computing Simulation (HPCS)* 1030–1033 (2014).
837 doi:10.1109/HPCSim.2014.6903807.
- 838 94. Pettersen, E. F. *et al.* UCSF Chimera--a visualization system for exploratory research and
839 analysis. *J Comput Chem* **25**, 1605–1612 (2004).
- 840
- 841
- 842
- 843
- 844

Demographic Data		COVID-19 group		CONTROL group	
		Mean +/- SD	N (%)	Mean +/- SD	N (%)
Age		54.56 +/- 16.86		52.83 +/- 15.5	
Sex	male		14 (44%)		13 (41%)
	female		18 (56%)		19 (59%)
Mild-to moderate patients			22 (68.7%)		
Asymptomatic patients			10 (31%)		
Comorbidities	Hypertension		9 (28.1%)		7 (21.9%)
	Dementia		4 (12.5%)		1 (3.1%)
	Cardiovascular diseases		5 (15.625%)		5 (15.625)
	HCV infection		2 (6.3%)		0
	Anemia		2 (6.3%)		2 (6.3%)
	Encephalopathy		3 (9.4%)		0
	Adenomatous Polyposis Coli		2 (6.3%)		0

Fig.1

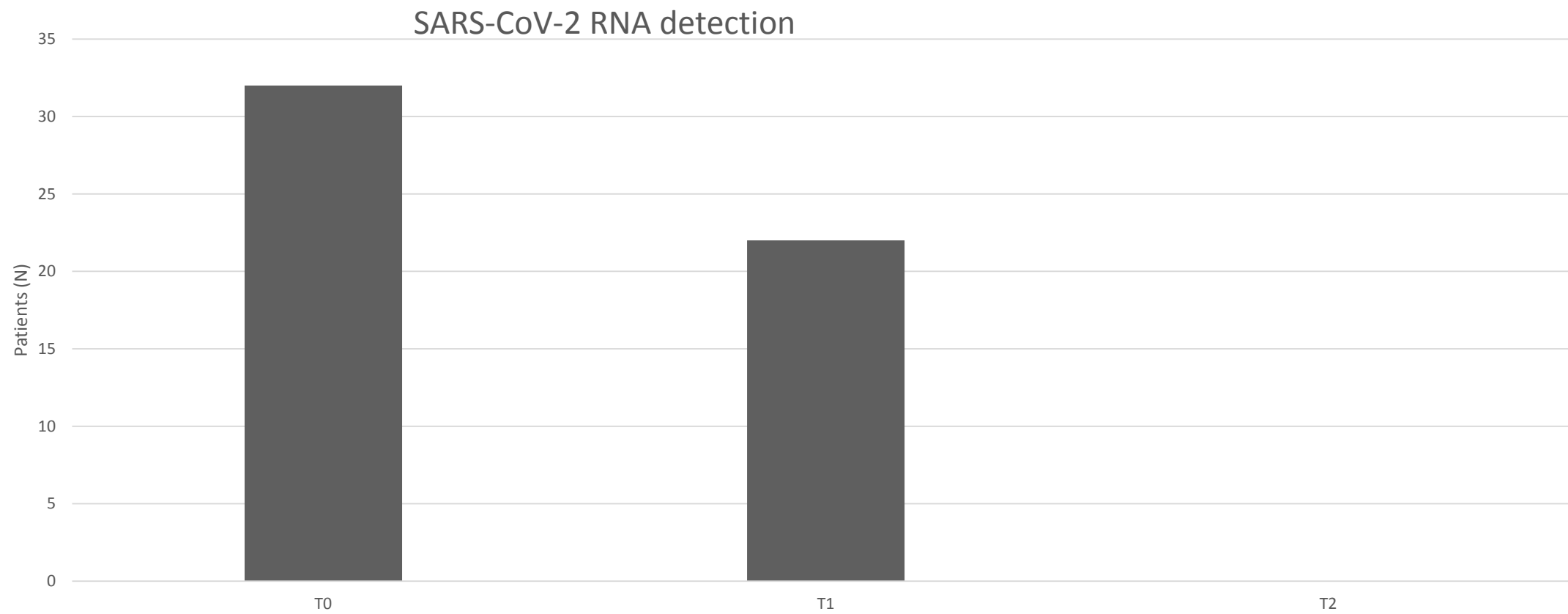


Fig.2

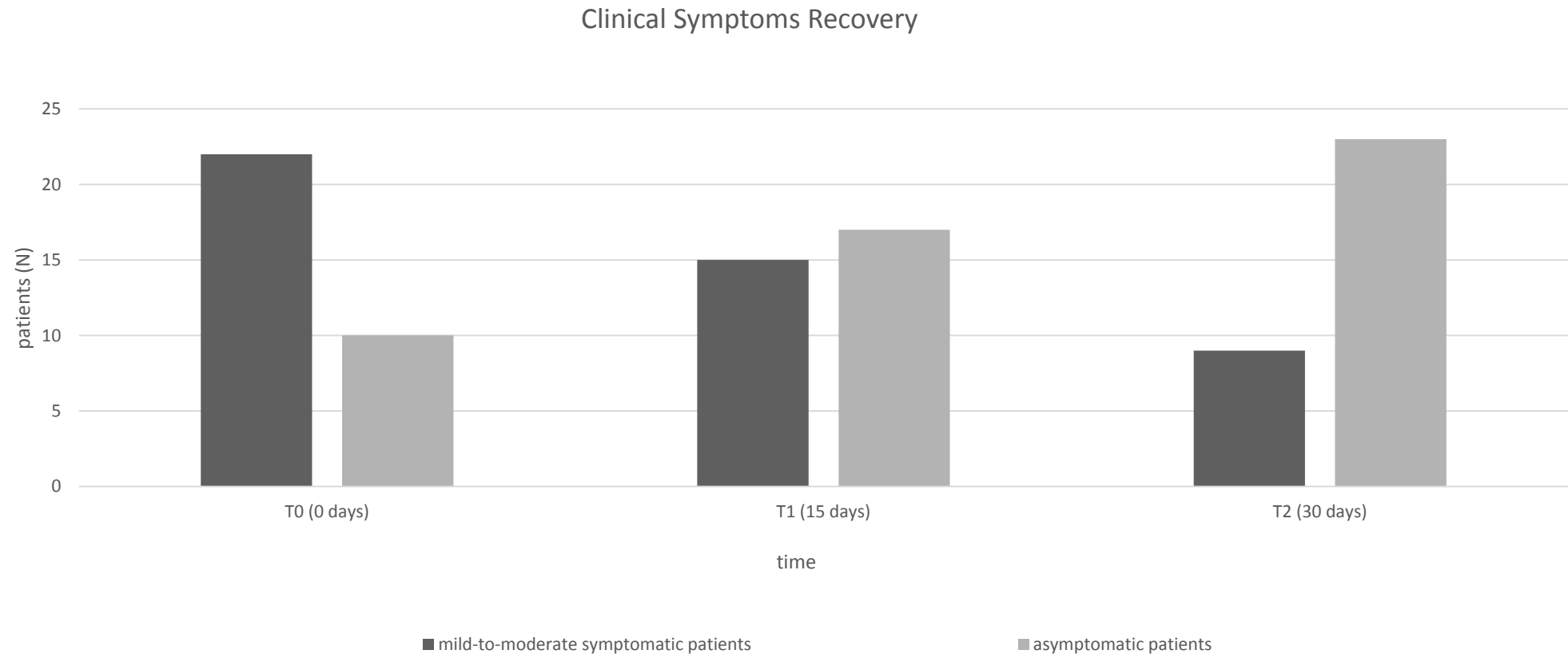


Fig. 3

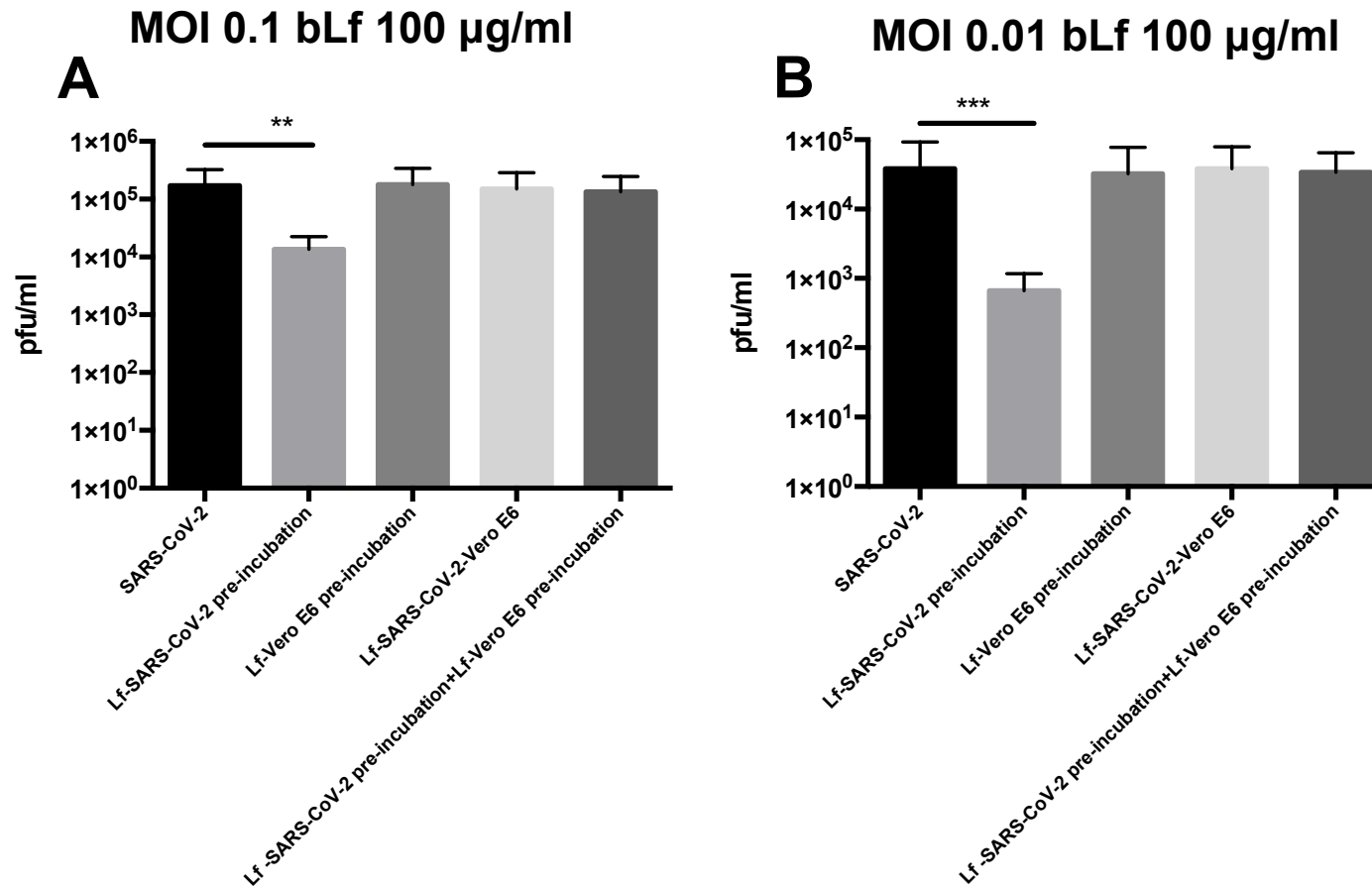


Fig. 4

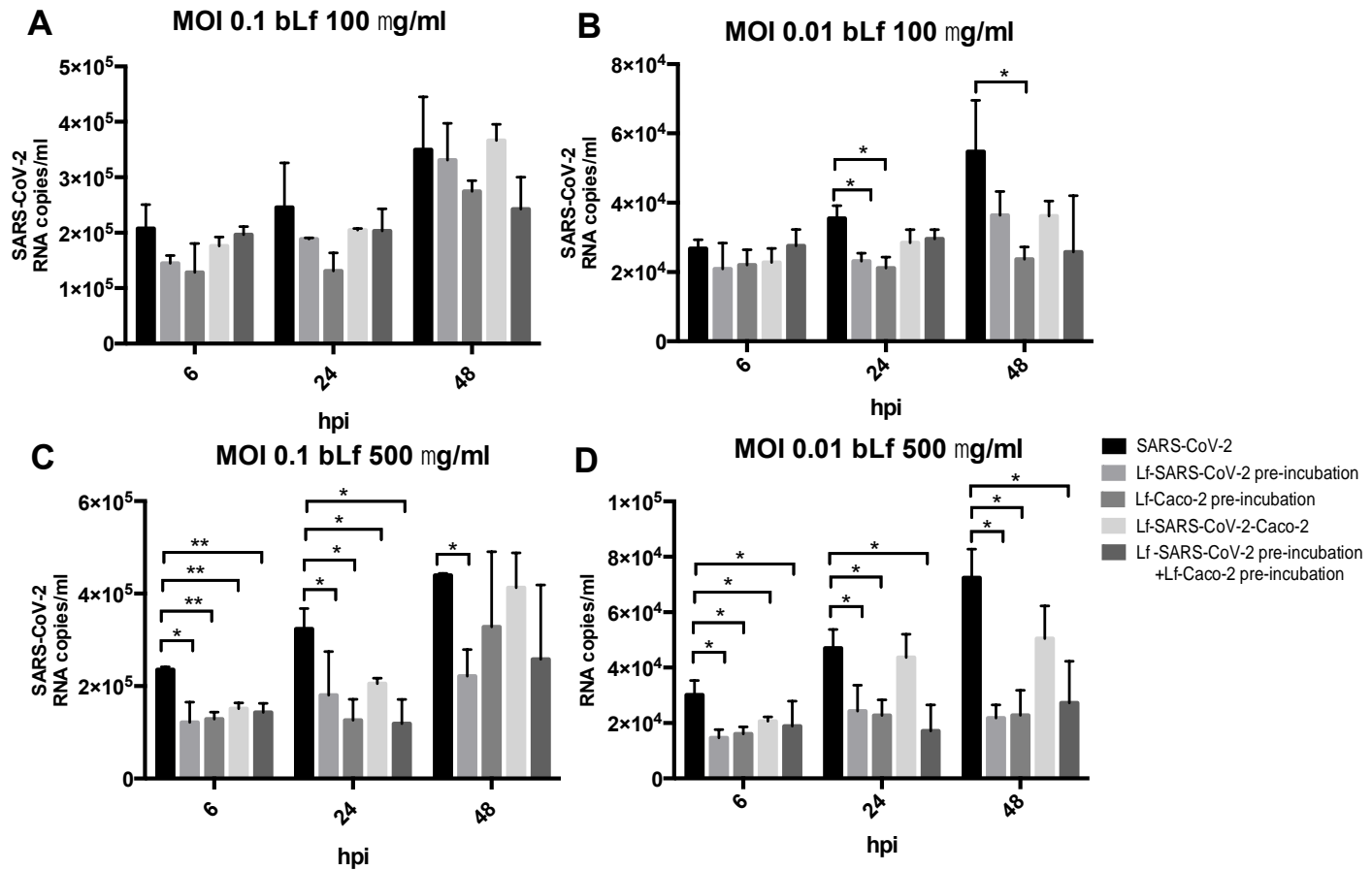


Fig. 5

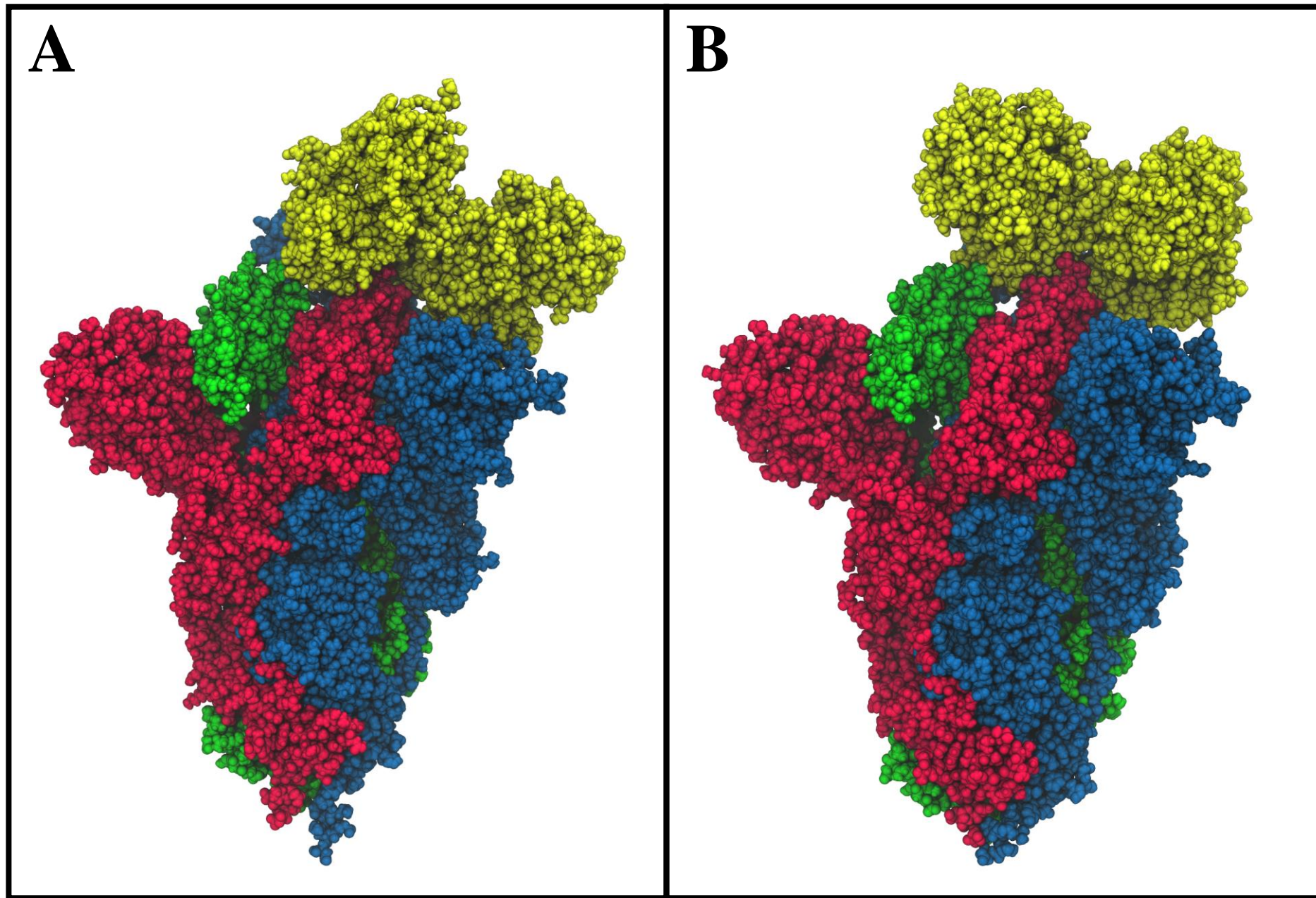


Fig. 6

